Identification and Characterization of a Novel Mutation in the Carbonic Anhydrase IV Gene that Causes Retinitis Pigmentosa

Bernardo V. Alvarez,[1,2] *Eranga N. Vithana,*[2,3] *Zhenglin Yang,*[2,4,5,6,7] *Adrian H. Koh,*[8] *Kit Yeung,*[3] *Victor Yong,*[3] *Haley J. Shandro,*[9] *Yali Chen,*[4] *Prasanna Kolatkar,*[10] *Paaventhan Palasingam,*[10] *Kang Zhang,*[4] *Tin Aung,*[3,8,11] *and Joseph R. Casey*[1,9]

Purpose. The autosomal dominant retinitis pigmentosa (adRP) gene on chromosome 17, region q22 (RP17), was recently identified as a glycosylphosphatidylinositol membrane-anchored zinc metalloenzyme (protein CAIV), highly expressed in the choriocapillaris of the eye and undetectable in the retina. Only two missense mutations have thus far been identified in the gene *CA4*. Functional analysis of these mutations demonstrated that retinal disease may result from perturbation of pH homeostasis in the outer retina, after disruption of CAIV and sodium bicarbonate cotransporter 1 (NBC1)–mediated bicarbonate transport. *CA4* was screened in a panel of patients with RP, to expand the mutation spectrum of this novel adRP gene and understand its pathogenic mechanism.

Methods. A total of 96 patients with simplex RP and adRP of Chinese ethnicity were screened for mutations in the eight coding exons of the *CA4* gene by bidirectional sequencing. Functional consequences of *CA4* mutations on the NBC1-mediated bicarbonate transport were studied by measuring bicarbonate fluxes in HEK293 cells cotransfected with NBC1 and *CA4* mutant cDNAs.

Results. Thirteen sequence alterations were identified, including a novel mutation within exon 3 of *CA4* (R69H) in a patient with simplex RP. R69H was not found in 432 normal chromosomes. R69H CAIV impaired NBC1-mediated pH recovery after acid load.

Conclusions. A novel mutation has been identified in *CA4* that provides further evidence that impaired pH regulation may underlie photoreceptor degeneration in RP17. This study indicates that, as with European patients with RP, mutations in *CA4* also account for ≤1% of Chinese patients with RP. (*Invest Ophthalmol Vis Sci.* 2007;48:3459–3468) DOI:10.1167/iovs.06-1515

Retinitis pigmentosa (RP) is a heterogeneous group of retinal dystrophies, characterized by degeneration of photoreceptor cells in the peripheral retina. RP leads to night blindness and visual field loss, which may progress to complete blindness later in life (for a review, see Ref. 1). With an incidence of ~1 in 3500, RP can be inherited as an X-linked, autosomal dominant, or autosomal recessive condition. Autosomal dominant (ad)RP is caused by mutations in 15 known genes.[2] The occurrence of adRP families, in which all known RP genes have been excluded, implies further genetic heterogeneity. The most recently cloned adRP gene is the *CA4* gene on chromosome 17, region q22 (RP17).[3,4]

Carbonic anhydrase 4 (*CA4* is the gene and CAIV the protein), encodes a glycosylphosphatidylinositol (GPI) membrane-anchored zinc metalloenzyme, expressed on the luminal surface of microcapillaries, that is highly expressed in the choriocapillaris of the eye.[5,6] The CAIV isozyme is also found on the luminal surface of epithelial cells in specific segments of the renal tubule, colon, gall bladder, and epididymis and on the luminal surface of pulmonary endothelial cells.[7] CAIV catalyzes the reversible hydration of carbon dioxide ($H_2O + CO_2 \leftrightarrow HCO_3^- + H^+$). Because CAIV protein is not detectable in the retina, it is another example of a non–retina-specific gene implicated in a retinal disease.[8–11]

The outer retina contains the photoreceptors whose extremely high metabolic requirements lead to the production of copious acidic metabolites, including carbon dioxide and lactic acid, from aerobic and anaerobic respiration. Removal of this metabolic waste load presents a physiological challenge, since the retina is avascular. Yet, efficient removal of the retina and retinal pigment epithelium (RPE) acid load to maintain pH homeostasis is a critical function mediated by the choriocapillaris in the choroid. Effective HCO_3^- shuttling requires the coordinated function of carbonic anhydrases and plasma membrane bicarbonate transporters, moving bicarbonate across multiple cell layers, ultimately to the circulatory system. Bicarbonate transporters expressed throughout the eye probably

From [1]Membrane Protein Research Group, Department of Physiology, and the [9]Department of Biochemistry, University of Alberta, Edmonton Alberta, Canada; the [3]Singapore Eye Research Institute, Singapore; the [4]Department of Ophthalmology and Visual Science and the [5]Program in Human Molecular Biology and Genetics, Eccles Institute of Human Genetics, University of Utah, Salt Lake City, Utah; the [6]Sichuan Provincial Medical Academy and [7]Sichuan Provincial People's Hospital, Sichuan, People's Republic of China; the [8]Singapore National Eye Centre, Singapore; the [10]Genome Institute of Singapore, Singapore; the [11]Department of Ophthalmology, National University of Singapore, Singapore.

[2]Contributed equally to the work and therefore should be considered equivalent authors.

Supported by National Eye Institute Grants R01EY14428, R01EY14448, core P30EY and GCRC M01-RR00064 (KZ); the following foundations: the Foundation Fighting Blindness, the Ruth and Milton Steinbach Fund, the Ronald McDonald House Charities, the Macular Vision Research Foundation, the Knights Templar Eye Research Foundation, the Grant Ritter Fund, the American Health Assistance Foundation, the Karl Kirchgessner Foundation, the Val and Edith Green Foundation, and the Simmons Foundation; the Canadian Institutes of Health Research (JRC); and the Singapore Eye Research Institute (ENV). BVA was supported by a postdoctoral fellowship from the Canadian Cystic Fibrosis Foundation. JRC is a Scientist of the Alberta Heritage Foundation for Medical Research.

Submitted for publication December 20, 2006; revised March 26, 2007; accepted May 23, 2007.

Disclosure: **B.V. Alvarez**, None; **E.N. Vithana**, None; **Z. Yang**, None; **A.H. Koh**, None; **K. Yeung**, None; **V. Yong**, None; **H.J. Shandro**, None; **Y. Chen**, None; **P. Kolatkar**, None; **P. Palasingam**, None; **K. Zhang**, None; **T. Aung**, None; **J.R. Casey**, None

The publication costs of this article were defrayed in part by page charge payment. This article must therefore be marked "*advertisement*" in accordance with 18 U.S.C. §1734 solely to indicate this fact.

Corresponding author: Joseph R. Casey, Department of Physiology and Department of Biochemistry, 721 Medical Sciences Building, University of Alberta, Edmonton, Alberta, Canada; joe.casey@ualberta.ca.

TABLE 1. Sequence Alterations Identified in *CA4*

(Exon/Intron)	DNA Change	Cases (%) (96)	Control (%)
5′ UTR	−24G>C	9 (9.4)	—
IVS1	IVS+72G>T	14 (14.6)	—
IVS1	IVS+145C>G	9 (9.4)	—
IVS1	IVS+82C>T	1 (1.0)	—
Exon 3	206G>A **(Arg69His)**	1 (1.0)	0/216
IVS 3	IVS3+78A>T	6 (6.3)	21/216 (9.7)
IVS 4I	IVS4−39C>G	2 (2.1)	
Exon 5	435A>G (Lys145Lys)	1 (1.0)	—
IVS 5	IVS5−79C>T	7 (7.3)	—
Exon 6	531C>A (Asn177Lys)	4 (4.2)	2/44 (4.4)
Exon 7	610C>T (Leu204Leu)	1 (1.0)	—
IVS 7	IVS7+18C>T	1 (1.0)	—
IVS 7I	IVS7−28G>T	1 (1.0)	—

IVS, intervening sequence; UTR, untranslated region.

serve to effect HCO_3^- efflux from the retina into the blood.[12–14] Functional interactions between carbonic anhydrase IV and the Na^+/bicarbonate cotransporter 1 (NBC1), also localized in the endothelium of the choriocapillaris in the plasma membranes, have also been identified.[4,15] Therefore, despite its lack of expression in the retina itself CAIV plays a critical role by maintaining the pH in the outer retina, which is important for the normal function of photoreceptors. Retinal phototransduction is modulated by pH changes in its surrounding environment.[16]

Thus far, only two missense mutations (R14W, R219S) have been identified in *CA4*.[3,4] Therefore, we screened this gene in our panel of Chinese patients with RP to identify novel mutations, to expand the mutation spectrum for *CA4*, and also to conduct functional studies for a better understanding of the disease mechanism underlying this form of RP.

METHODS

Patients

Written, informed consent was obtained from all patients. The study had the approval of the Ethics Committee of the Singapore Eye Research Institute and was performed according to the tenets of the Declaration of Helsinki. A detailed history was recorded for all subjects, focusing on the typical signs of RP and their onset. All patients underwent a complete ophthalmic examination including visual acuity testing, funduscopy, photodocumentation, Goldmann perimetry, dark-adaptation studies, and full-field electroretinography (ERG), in accordance with the International Society for Clinical Electrophysiology of Vision guidelines.[17]

Mutation Detection

Genomic DNA was extracted from leukocytes of the peripheral blood of the patients and exons 1 to 8 of the *CA4* gene were amplified by polymerase chain reaction (PCR) using established methods.[4] Sequences of oligonucleotide primers used have been published.[4] PCR products were purified using GFX PCR purification columns (GE Healthcare, Buckinghamshire, UK). Sequence variations were identified by automated bidirectional sequencing by dye termination chemistry (BigDye terminator ver. 3.1; Applied Biosystems, Inc. [ABI], Foster City, CA) and an automated DNA sequencer (Prism Model 3100; ABI). Primers for sequence reactions were the same as those for the PCR reaction.

Molecular Modeling

The structure of human CAIV (Protein Data Bank ID 1ZNC)[7] was used as a template to model both R219S and R69H mutations, using the Swiss-PDB Viewer application.[18] Arg219 of the wild-type enzyme was replaced with Ser219 and subjected to energy minimization comprising 50 steps of steepest descent with a cutoff for nonbonded interactions of 10 Å. Similarly, Arg69 was replaced with His69 and subjected to energy minimization using the same protocol.

Protein Expression

HEK293 cells were cotransfected with 2 μg of human NBC1 cDNA[19] and 1 μg of either wild-type CAIV or mutant CAIV-R69H cDNA,[4] by the calcium phosphate transfection method.[4] Both CAIV variant cDNAs were cloned into the pcDNA3 vector. Carrier DNA (empty pcDNA3) was added so that DNA in each transfection totaled 3 μg. To examine the effect of CAIV mutants on NBC1 activity, NBC1 was coexpressed with wild-type and mutant CAIV cDNAs. Transport rates were assessed for the transfected cells, as described subsequently. For confocal experiments, HEK293 cells were also transfected with human SLC26A6 cDNA.[20]

Immunoprecipitation

HEK293 cells transiently transfected with NBC1 cDNA or pcDNA3.1 alone, transfected or cotransfected with NBC1 and CAIV-WT or with NBC1 and CAIV-R69H, cDNAs, were grown in 100 tissue culture plates, for 48 hours. The cells were washed with PBS (140 mM NaCl, 3 mM KCl, 6.5 mM Na_2HPO_4, 1.5 mM KH_2PO_4 [pH 7.5]) and harvested by lysis in 500 μL of IPB buffer (1% [vol/vol] NP40, 5 mM EDTA, 150 mM NaCl, 0.5% [wt/vol] sodium deoxycholate, 10 mM Tris-HCl [pH 7.50]), and protease inhibitor cocktail (MiniComplete Tablet; Roche, Indianapolis, IN). Lysates were clarified by centrifugation at 16,300*g* for 15 minutes at 4°C. Samples were immunoprecipitated with 2 μL of goat anti-CAIV antibody (N-16; Santa Cruz Biotechnology, Santa Cruz, CA), using a protocol described previously.[15] Immunoprecipitates

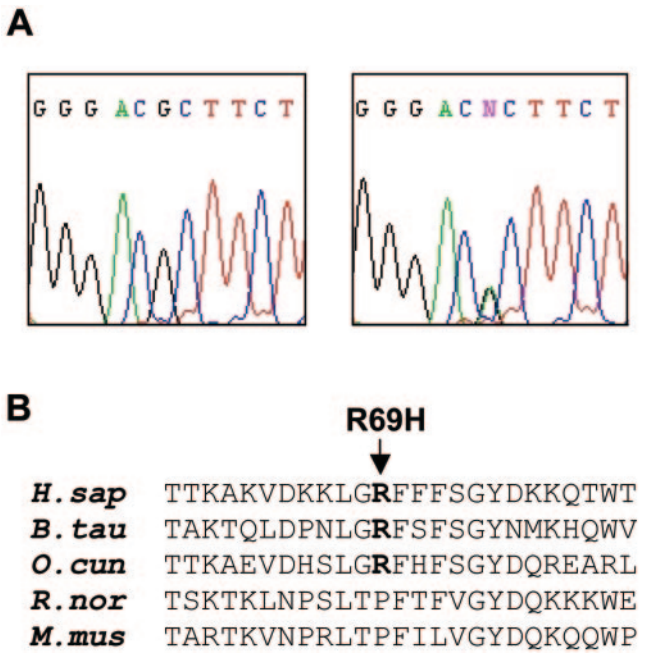

FIGURE 1. Mutation of *CA4* identified in the Chinese RP patient. (**A**) The wild-type sequence (*left*) and mutant *CA4* sequence (*right*) depicting the G→A transition that changed codon 69 from arginine (CGC) to histidine (CAC). The mutated position is marked N, indicating a sequence mixture at this position. This reflects the patient's heterozygous genotype, with G on one allele and A on the affected allele. (**B**) Amino acid sequence alignment of residues 58 to 82 of human (*Homo sapiens*) CAIV compared with orthologs from other species: bovine (*Bos taurus*), rabbit (*Oryctolagus cuniculus*), rat (*Rattus norvegicus*), and mouse (*Mus musculus*).

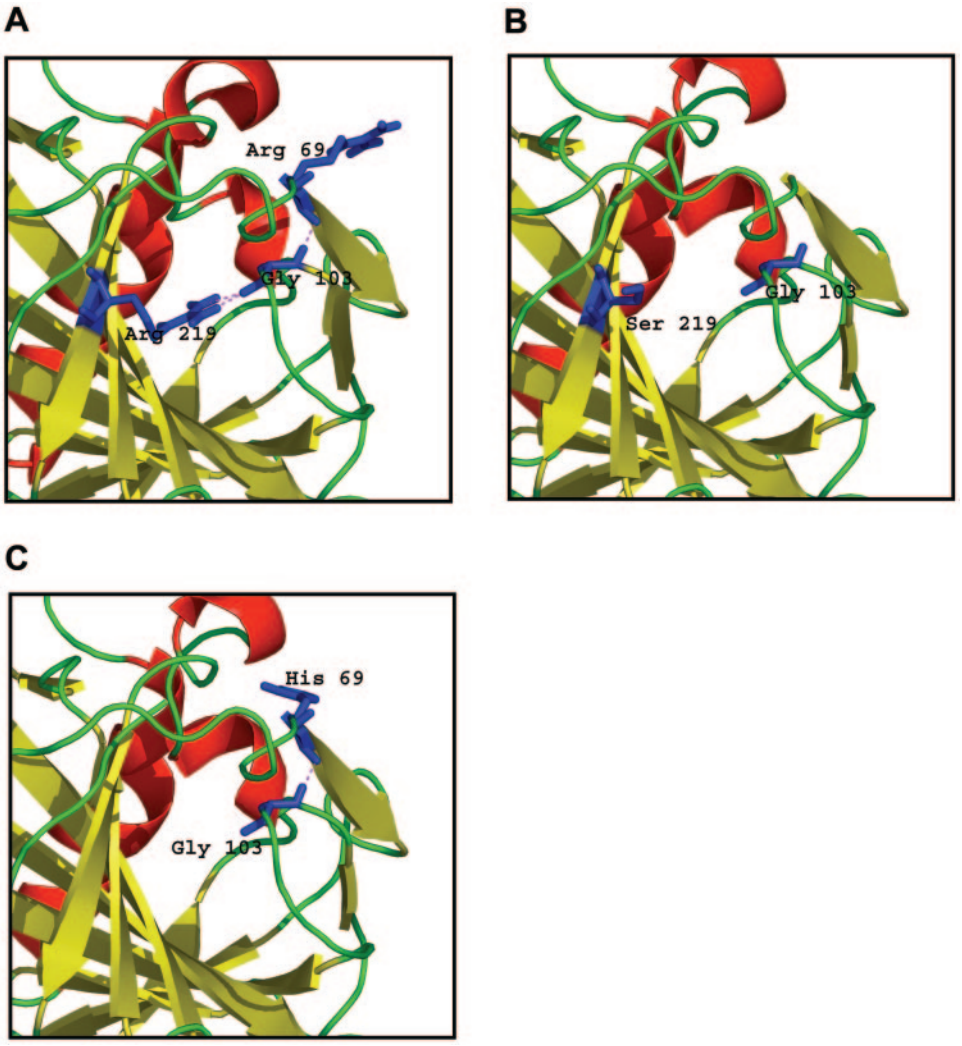

FIGURE 2. Structural model for the mutated region of human CAIV protein. β-Sheets are shown as *yellow* ribbons and α-helix is in *red*. (**A**) The native CAIV structure shows that the Gly103-containing loop interacts with both R219 and R69, mutated individually in patients with RP. The carbonyl moiety of Arg69 forms a hydrogen bond with amide of Gly103, whereas the NH1 and the NH2 atoms of the Arg219 side chain form hydrogen bonds with the carbonyl of Gly103. (**B**) Substitution of Arg219 with serine disrupts these hydrogen bonds with Gly103. (**C**) The modeled structure of R69H shows that His69 retains a hydrogen bond with the main chain of Gly103, mimicking the wild-type structure. Hydrogen bonds are colored with magenta. Structures were rendered with PyMOL software.[29]

were analyzed on immunoblots, probed with rabbit anti-NBC1 antibody,[15] or rabbit anti-CAIV antibody.[4]

Immunoblot Analysis

Samples (10 μg protein) were resolved by SDS-PAGE on 8% acrylamide gels. Proteins were transferred to PVDF membranes and then incubated with either rabbit anti-NBC1[4] or goat anti-CAIV antibody (Santa Cruz Biotechnology). Immunoblots were incubated with donkey anti-rabbit IgG conjugated to horseradish peroxidase, or rabbit anti-goat IgG conjugated to horseradish peroxidase.[21] Blots were visualized and quantified by using chemiluminescence and an imaging station (Eastman-Kodak, Rochester, NY).

GST Pull-Down Assays

Blot overlay assays to detect interactions of GST fusion proteins with CAIV-WT and CAIV-R69H mutant were performed as previously described.[15,21] Fusion proteins corresponding to the fourth extracellular loop (amino acids 643-677) of AE1 (GST-AE1EC4) or corresponding to the third extracellular loop (amino acids 603-689) of NBC1 (GST-NBC1EC3) or the fourth extracellular loop (amino acids 748-779) of NBC1 (GST-NBC1EC4) have been described.[15,21] Briefly, HEK293 cells grown in 100-mm culture dishes were transiently transfected individually with cDNA encoding CAIV-WT, or CAIV-R69H mutant. Untransfected HEK293 cells, or cells individually expressing CAIV-WT or CAIV-R69H mutant, were solubilized in 1 mL IPB buffer, supplemented with protease inhibitors (Mini Complete tablets; Roche), and applied to GST fusion expression constructs (250 μg) on glutathione-Sepharose resins and incubated overnight. Samples were then centrifuged and washed four times with a washing buffer (0.1% [vol/vol] NP40, 150 mM NaCl, 1 mM EDTA, 10 mM Tris [pH 7.5]). Immunoblots of fusion proteins were prepared as previously described.[15] The immunoblots were blocked for 2 hours with 10% TBST-M buffer (TBST buffer containing 0.1% [vol/vol] Tween-20, 137 mM NaCl, 20 mM Tris [pH 7.5]) containing 5% [wt/vol] nonfat dry milk), then washed three times for 5 minutes each in TBST and then probed for CAIV and GST, as described previously.[15,21]

Cell Surface Processing Assays

Assays to assess the degree of cell surface processing and biotinylation of CAIV-WT and CAIV-R69H mutant were performed, as described previously.[4]

Assay of NBC1 Activity

HEK293 cells were grown on poly-L-lysine–coated glass coverslips. The cells were transfected with NBC1 alone, cotransfected with NBC1 and wild-type CAIV, cotransfected with NBC1 and CAIV-R69H mutant, or cotransfected with NBC1 and a combination of wild-type CAIV and CAIV-R69H mutant cDNAs. Initial rates of pH_i recovery from an acid load were calculated by linear regression of the first minute of the pH_i recovery after maximum acidosis,[4] (Kaleidagraph Software; Synergy Software, Reading, PA). In all cases, the transport activity of sham-

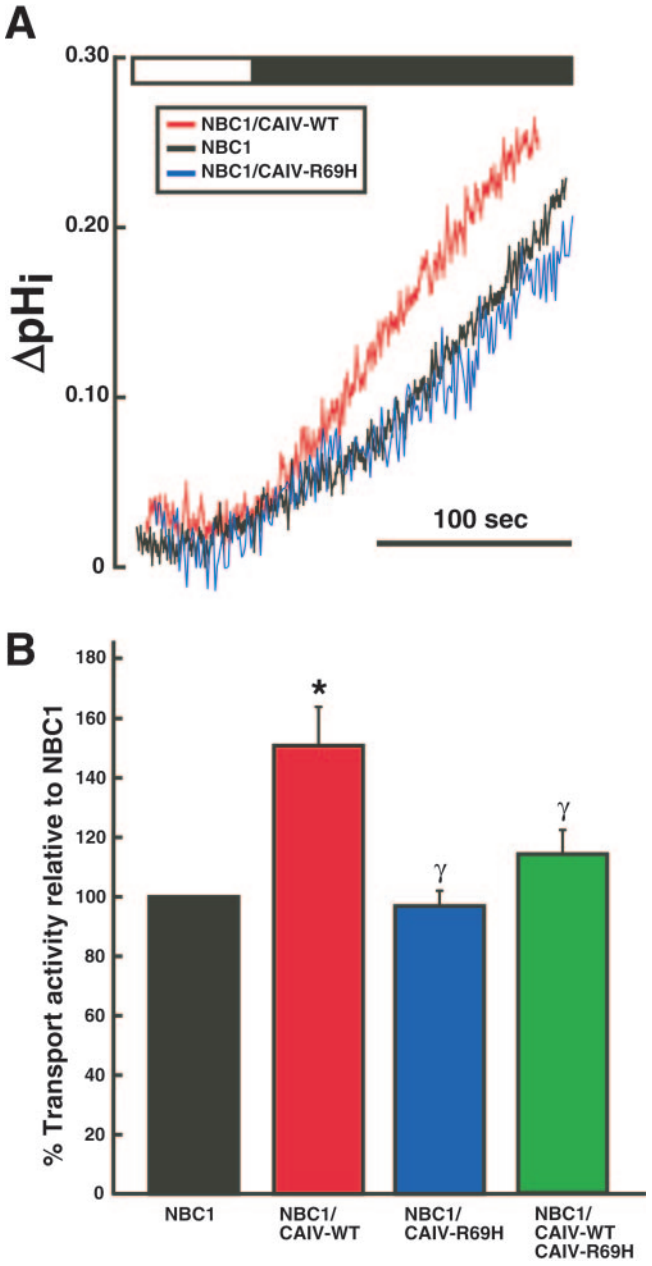

FIGURE 3. Effect of wild-type CAIV and CAIV-R69H on NBC1-mediated pH_i recovery. (**A**) Representative traces of pH_i recovery in HEK293 cells transfected with NBC1, NBC1 and CAIV-WT, or NBC1 and CAIV-R69H (see key). Acidification in NH_4Cl (30 mM □) was followed by NBC1-mediated pH_i recovery in bicarbonate-containing buffer (■). (**B**) Overall results of transport activity of cells transfected with cDNAs indicated at the bottom. NBC1 alone was set at 100%, and all other data were expressed relative to this value. *Significant difference ($P < 0.05$), compared with NBC1 alone. γ, significant difference ($P < 0.05$), compared with NBC1 coexpressed with WT-CAIV ($n = 4$ in each group).

transfected cells was subtracted from the total rate, to ensure that these rates consisted only of NBC1 transport activity.

CAIV Activity Assays

The assay procedure incorporated aspects from protocols described previously.[22–25] HEK293 cells transfected with empty vector, wild-type CAIV, CAIV-R219S mutant, or CAIV-R69H mutant cDNAs were removed from 60-mm dishes by cell scraping. Cell pellets were resuspended in 500 μL of 0.2% SDS in 5 mM Tris/SO_4 (pH 7.5), containing protease inhibitors (Mini-Complete; Roche). DNA in samples was sheared by repeated passage through a needle and syringe and incubated for 30 minutes at room temperature before assay. Unlike other CAs, CAIV is resistant to SDS denaturation, so that this assay reports only on CAIV enzymatic activity.[26] All assay reagents were chilled in an ice bath before use. In each assay, 3 mL H_2O was bubbled with 600 mL/min CO_2 gas for 1 minute. Cell lysate (100 μL) was added, followed by 3 mL of TI buffer (5 mM Tris and 20 mM imidazole [pH 9.4–9.9]). Assays were performed in glass test tubes in an ice-water bath on a magnetic stirrer with continuous stirring and CO_2 gassing throughout the experiment. Recordings of pH as a function of time were initiated on addition of TI buffer. CA activity was determined by linear regression of the rate of change of pH over a range of pH 7.5 to 7.0. The rate of change of pH in control samples (100 μL of 0.2% SDS in 5 mM Tris/SO_4 [pH 7.5]) was subtracted from each of the rates. Activity of CAIV/mg total protein was determined by dividing the corrected activity by expression of protein in the samples (BCA assay). CAIV activity was corrected for CAIV expression by immunoblot analysis.

Confocal Microscopy

Cells grown on 22-mm^2 poly-L-lysine–coated coverslips were transiently transfected as described earlier. The cells were washed in PBS and fixed for 20 minutes in 3.5% (wt/vol) paraformaldehyde in PBSCM (PBS containing 1 mM $CaCl_2$ and 1 mM $MgCl_2$). The cells were washed with PBS and incubated for 2 minutes in PBS containing 0.1% (vol/vol) Triton X-100. The slides were blocked for 25 minutes with 0.2% (wt/vol) gelatin in PBS and incubated with a 1:1000 dilution of goat anti-CAIV antibody (N-16; Santa Cruz Biotechnology) and rabbit polyclonal anti-NBC1 antibody (clone B5, 1:100 dilution; Proteus Biosciences Inc., Ramona, CA), or of anti-SLC26A6 antibody (1:1000; N-terminal antibody[27]) and goat iron-transporter receptor (TfR) antibody (1:1000 hCD71-C20; Santa Cruz Biotechnology), for 1 hour in a humidified chamber at room temperature. The slides were processed and images collected as described.[20] The images were quantified by commercial software (MetaMorph; Molecular Devices, Sunnyvale, CA), with saturation at 50% intensity. The software compared the images (NBC1 and either CAIV-WT or CAIV-R69H, or SLC26A6 and TfR signal) pixel by pixel and determined the percentage of overlapping of the fluorescent signals.

RESULTS

Mutation Analysis

A total of 96 subjects of Chinese ethnicity who had RP were studied, resulting in the identification of 13 *CA4* sequence alterations (Table 1). Of these, the G→A transition mutation in exon 3 that resulted in the substitution of amino acid arginine for histidine at codon 69 (R69H) was identified in a single patient with sporadic RP who had no prior family history of RP (Fig. 1A). This change was not found in 432 ethnically matched control chromosomes, strongly supporting pathogenicity. Alignment of amino acid sequences of CAIV from several mammalian species by CLUSTAL-W[28] revealed that either arginine or proline, but never histidine, was at amino acid position 69 (Fig. 1B). All other sequence changes have either been reported earlier as benign polymorphisms or have been found in control individuals.

The patient concerned was an 11-year-old boy who presented with nyctalopia and poor vision since the age of 3 years. Visual acuity was 20/200 in both eyes, and visual fields were severely constricted (<10°). Fundus examination revealed bilateral pigment clumping at the level of retinal pigment epithelium, without the typical bone spicule pigmentation appearance of RP. Electroretinography recordings (ERG) showed no observable rod- or cone-derived ERG responses, indicating panretinal dysfunction of retinal photoreceptors.

TABLE 2. Experimental Parameters during Analysis of NBC1 Transport Activity

Parameter	NBC1/CAIV-WT	NBC1/CAIV-R69H
Steady-state pH_i (HEPES buffer)	7.50 ± 0.10	7.49 ± 0.08
Steady-state pH_i (HCO_3^- buffer)	7.22 ± 0.04	7.13 ± 0.03*
Maximum acidosis (HEPES to HCO_3^-)	6.90 ± 0.04	6.84 ± 0.03
β_{int} (mM)	2.67 ± 0.43	3.62 ± 0.81
β_{tot} (mM)	20.85 ± 1.90	18.69 ± 1.01
$[HCO_3^-]_i$ (mM)	7.90 ± 0.80	6.60 ± 0.30
$\Delta pH_i \cdot min^{-1}$	0.093 ± 0.021	0.063 ± 0.009*
$J_{HCO_3} \cdot (mM \cdot min^{-1})$	1.74 ± 0.31	1.14 ± 0.16*

HEK293 cells were transfected with cDNA encoding NBC1 and wild-type CAIV, or NBC1 and R69H-CAIV. The cells were analyzed for buffer capacity, as previously described.[31,32] Steady state pH_i (HEPES buffer) was measured in cells stabilized in HEPES-buffered, bicarbonate-free Ringer's buffer. They were then acidified by switching to bicarbonate/CO_2-containing Ringer's buffer and maximum acidosis (HEPES to HCO_3^-) was measured. The rate of recovery of pH_i was then measured as $\Delta pH_i \cdot min^{-1}$. J_{HCO_3} was calculated as: $(\Delta pH_i \cdot min^{-1}) \times \beta_{tot}$. β total (β_{tot}) is the sum of intrinsic buffering capacity (β_{int}) plus buffering capacity due to CO_2/HCO_3^- (β_{CO_2}). $[HCO_3]_i$ was estimated according to the Henderson-Hasselbach equation. Data represent the mean ± SE of five experiments.

* $P < 0.05$, comparing CAIV-WT to CAIV-R69H.

Protein Modeling of the Mutations

The structure wild-type CAIV revealed that Arg69 resides in a β-strand region that facilitates structural integrity via hydrogen bond formation to the residue, Gly103, residing in an adjacent loop[7] (Fig. 2A). Of interest, another CAIV mutation that causes RP, R219S[4] is in a separate β-strand region (Fig. 2A). Although Arg69 is located on the surface of CAIV, Arg219 is located at the active cleft of the enzyme. The carbonyl of Arg69 forms a hydrogen bond with the amide of Gly103, whereas the NH1 and the NH2 atoms of the Arg219 side chain form hydrogen bonds with the carbonyl of Gly103. Hydrogen bond analysis of the mutant model R219S revealed that Ser219 does not form a hydrogen bond with Gly103 (Fig. 2B). The modeled structure of R69H-CAIV predicts that His69 retains a hydrogen bond with main chain Gly103, thus mimicking the wild-type structure and preserving the local tertiary structure (Fig. 2C). This modeling, however, does not take into account possible changes in hydrogen bonding resulting from the main chain atoms.

Effect of Mutant CAIV on HCO_3^- Flux through NBC1

High rates of metabolic waste H^+ production in the retinal epithelium are dissipated by the blood flow in the choriocapillaris. Carbonic anhydrases, working along with bicarbonate transporters will funnel waste CO_2/HCO_3^- to the blood. Because NBC1 and CAIV colocalize in choriocapillaris, it is likely that their association contributes to essential HCO_3^- flow from retina to blood. The functional association of CAIV and NBC1 in the endothelium of choriocapillaris facilitates the elimination of acid production. Rapid catalysis of CO_2/HCO_3^- in the plasma membrane mediated by CAIV maximizes the transmembrane HCO_3^- gradient and increases the NBC1-mediated HCO_3^- transport rate.[4,15]

We investigated the effect of the identified R69H *CA4* mutation on NBC1-mediated HCO_3^- transport in HEK293 cells cotransfected with NBC1 and CAIV-R69H mutant cDNAs. Cells were loaded with 2′,7′-*bis*(2-carboxyethyl)-5(6)-carboxyfluorescein-acetoxymethyl ester (BCECF-AM) fluorescent dye, to monitor intracellular pH (pH_i). The bicarbonate flux associated with these cells was determined as ΔpH_i/min, after exposing the cells to acid load, using the NH_4Cl pulse technique.[30] Amiloride-insensitive pH_i recovery after acid load is attributable to NBC1 activity (Fig. 3). The transport rate for HEK293 cells cotransfected with NBC1 and CAIV cDNA was significantly higher when compared with cells expressing only NBC1 (Fig. 3A). Coexpression of wild-type NBC1 and CAIV-R69H mutant proteins failed to increase the rates of pH_i recovery after acid load, relative to NBC1 alone (Fig. 3A). In contrast, coexpression of NBC1 and wild-type CAIV increased NBC1-mediated HCO_3^- transport by 41% ± 16% ($n = 4$; Fig. 3B). Expression of CAIV-R69H mutant did not, however, increase HCO_3^- transport by NBC1, when compared with cells expressing NBC1 alone ($n = 4$; Figs. 3A, 3B). The initial decline in pH_i was similar in all three groups, reaching an acid load peak of 6.53 ± 0.03 (NBC1), 6.55 ± 0.03 (NBC1/CAIV-WT), and 6.53 ± 0.07 (NBC1/CAIV-R69H; $n = 4$; one-way ANOVA). To mimic the heterozygous genotype of the patient with the R69H mutation, HEK293 cells were cotransfected with NBC1 and equivalent amounts of wild-type and R69H-CAIV. Intermediate pH_i recovery activity greater than for NBC1 with only R69H-CAIV, but less than NBC1 with WT CAIV was observed (activity 13% ± 7% above NBC1 alone, at pH_i 6.66 ± 0.07, $n = 4$).

We performed a series of additional experiments to explore the significance of these findings. A difference in rate of pH_i recovery in NBC1 expressing cells, coexpressing WT or R69H CAIV, could be explained whether the mutant CAIV-induced a change of the cell's buffer capacity (β). Table 2, however, reveals that $\beta_{intrinsic}$ did not differ significantly between cells expressing WT or R69H CAIV. To examine whether induction of acidosis using ammonium pulsing had unique effects on NBC1 activity, we also measured pH_i recovery in cells made acidotic by equilibration in nominally HCO_3-free HEPES solution, shifted to CO_2/HCO_3^- medium (Table 2). Steady state pH_i in the HEPES solution was not different between cells expressing WT or R69H CAIV with NBC1. Of interest, there was a significant difference in the steady state pH_i on shifting to HCO_3^- medium. The 0.09 pH unit reduction in pH_i in cells expressing R69H CAIV suggests that cells expressing mutant CAIV could manifest a defect in acid handling. Finally, consistent with the findings in the ammonium-pulsing experiments described earlier, the rate of NBC1-mediated pH_i recovery from CO_2/HCO_3^--induced acidosis was defective in cells expressing R69H CAIV relative to WT CAIV (Table 2), to a degree similar to that found in the ammonium-induced acidosis experiments.

Failure to activate NBC1 could be explained if the CAIV-R69H mutant was insufficiently expressed at the cell surface. To determine whether the CAIV-R69H mutant expression varies from wild-type CAIV, we performed cell surface processing assays. HEK293 cells expressing wild-type and mutant CAIV were exposed to a membrane-impermeant biotinylation reagent (EZ-Link Sulfo-NHS-SS-Biotin; Pierce Biotechnology,

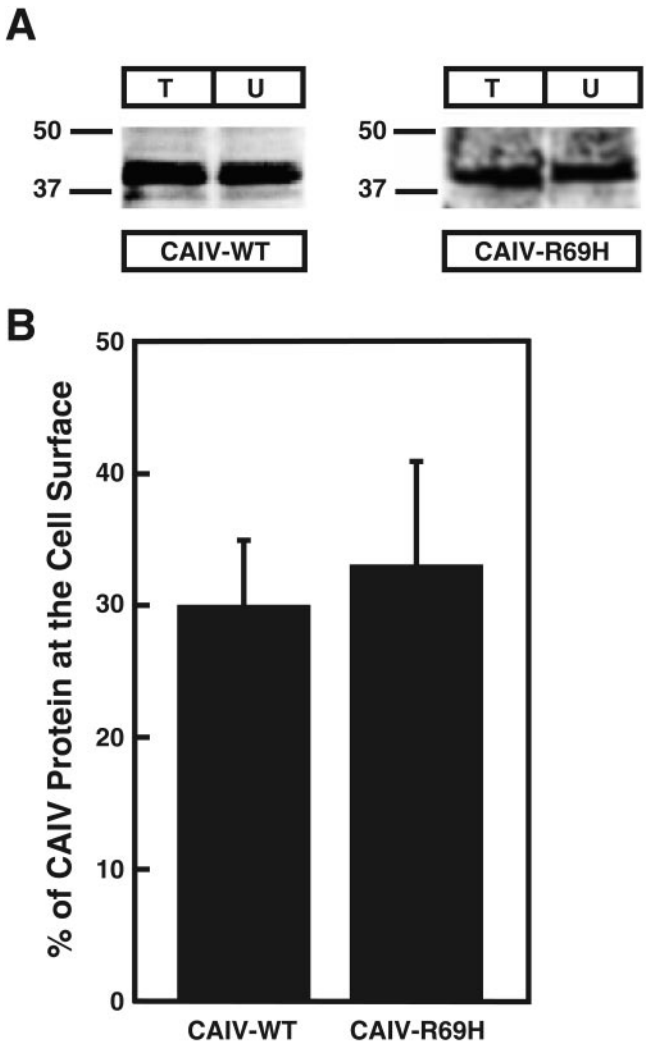

FIGURE 4. Cell-surface expression of CAIV-WT and CAIV-R69H mutant. (**A**) HEK-293 cells, individually transfected with CAIV-WT or CAIV-R69H mutant cDNA, were incubated with a membrane-impermeant, amine-directed compound (EZ-Link Sulfo-NHS-SS-Biotin; Pierce Biotechnology, Rockford, IL). Cells were solubilized, and proteins were incubated with streptavidin resin. Biotinylated proteins associated with the resin were eluted with SDS-PAGE sample buffer. Protein samples (T, total; U, unbound; and E, eluted fractions) were electrophoresed on polyacrylamide gels and transblotted to PVDF membrane. Blots were developed using anti-CAIV antibody, incubated with chemiluminescence reagent and imaged. (**B**) The fraction of CAIV associated with the plasma membrane was quantified by densitometry of the immunoblotted proteins and calculated as [(total − unbound)/total] × 100%; n=3.

Rockford, IL). Biotin-labeled proteins at the surface of the cell will bind to streptavidin resin. The amount of total and streptavidin resin-bound wild-type CAIV and CAIV-R69H mutant was assessed on immunoblots (Fig. 4). Quantification of the amount of biotinylated CAIV protein revealed that CAIV-R69H mutant was processed to the cell surface to a degree indistinguishable from wild-type CAIV (n = 3, Fig. 4B). These data show that only approximately 30% of each of the proteins was biotinylated and thus cell surface associated. Therefore, a great portion of each protein was retained in intracellular membranes during biosynthesis.

Unlike CAIV-R219S, a mutation previously described with no catalytic activity, we found that recombinant CAIV-R69H is catalytically active (Table 3), when compared with wild-type CAIV. There was a small, but statistically insignificant decrease in CAIV-R69H, relative to WT-CAIV. This result suggests that CAIV-R69H failed to increase NBC1-mediated HCO_3^- fluxes by disruption of metabolon formation rather than altered CA activity. To examine this hypothesis, we performed coimmunoprecipitation, GST pull-down, and colocalization studies.

Coimmunoprecipitation of CAIV and NBC1

The association of transiently expressed CAIV with NBC1 was further assessed in immunoprecipitates (Fig. 5). The amount of CAIV-WT and CAIV-R69H mutant associated with NBC1 was quantified on immunoblots. CAIV-WT bound NBC1 (Fig. 5, top), but CAIV-R69H did not (Fig. 5, top). Cells transiently transfected with empty vector (pcDNA3), or NBC1 alone showed no nonspecific binding (Fig. 5, top). In a parallel blot, CAIV-WT and CAIV-R69H showed similar expression levels in lysates of HEK293 cells transiently transfected with CAIV-WT or CAIV-R69H and NBC1 (Fig. 5, bottom). Taken together, the data suggest that the binding of CAIV-R69H to NBC1 is somehow impaired.

GST Pull-Down Assays of CAIV and Extracellular Loops of NBC1

CAIV, anchored by a GPI-linker to the plasma membrane, faces the extracellular milieu where it interacts with the fourth extracellular region (EC) of the AE1 anion exchanger (AE1-EC4)[21] and the fourth extracellular region of the NBC1 cotransporter (NBC1-EC4).[15] In contrast, the third extracellular loop of NBC1 (NBC1-EC3) was found not to interact with CAIV.[15] In our study, GST fusion proteins of NBC1 EC3 (amino acids 603-689 of NBC1) and EC4 (amino acids 748-779 of NBC1) were used in GST pull-down assays. GST alone and GST fusion protein of EC4 of AE1 (GST-AE1EC4) were also used as negative and positive control samples, respectively, in GST-pull-down assays (Fig. 6A). GST fusion proteins were immobilized on glutathione resin. The resin was incubated with lysates prepared from sham-transfected HEK293 cells, or HEK293 cells expressing CAIV-WT or CAIV-R69H. The amount of CAIV associated with each fusion protein was assayed on immuno-

TABLE 3. Carbonic Anhydrase IV Enzymatic Activity

Cell Lysate Source	SDS-Resistant CA Activity (μmol/(min · mg) Total Protein)	Wild-Type Activity (%) (Normalized to CAIV Expression)
Vector-transfected cells	14 ± 4*	0*
Wild-type CAIV	488 ± 37	100
CAIV-R219S	24 ± 5*	5*
CAIV-R69H	388 ± 20	84

Data are expressed as the mean ± SE of results in five to six different trials.
* $P < 0.05$ relative to wild-type CAIV.

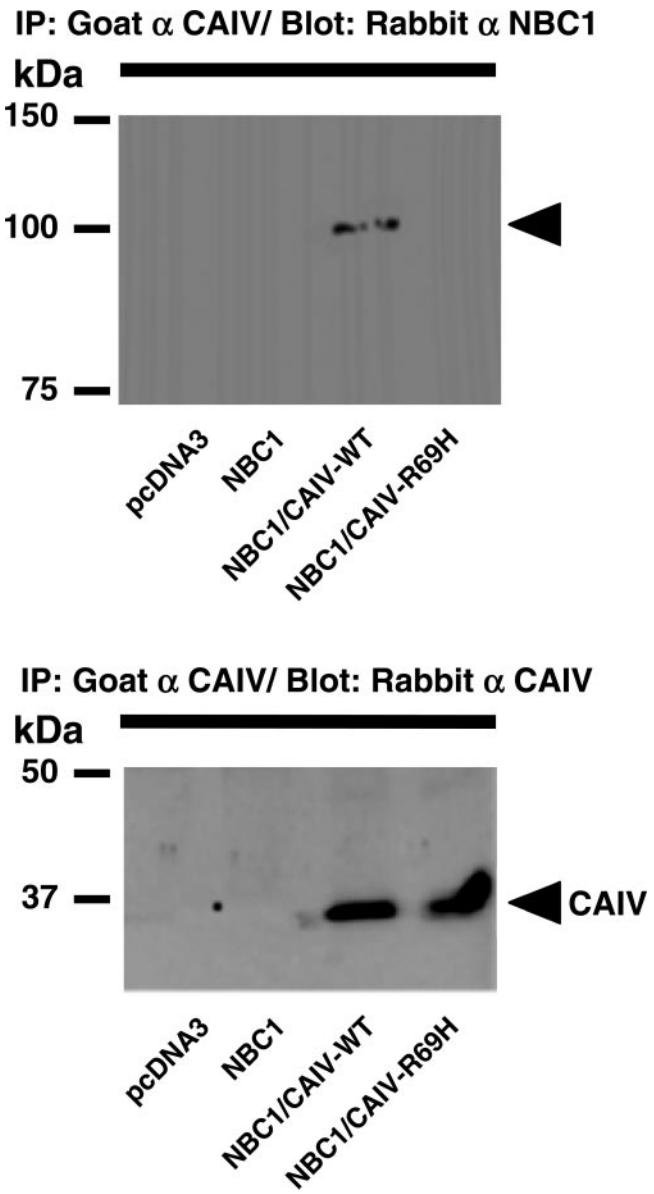

FIGURE 5. Coimmunoprecipitation of CAIV and CAIV-R69H with NBC1. HEK293 cells were transfected with vector alone (pcDNA3), and NBC1, or cotransfected with NBC1 and wild-type CAIV, or NBC1 and CAIV-R69H mutant, as indicated. Whole cell lysates were immunoprecipitated with anti-CAIV antibody and immunoprecipitates were probed for associated NBC1 on immunoblots probed with anti-NBC1 antibody (*top*). The amount of CAIV present in each sample was assessed on parallel blots probed with anti-CAIV antibody (*bottom*).

blots. CAIV associated with each resin was normalized to the amount of GST on the resin (not shown).

CAIV antibody failed to detect CAIV protein associated with GST fusion proteins when lysates of untransfected HEK293 cells were used (Fig. 6A, top). Conversely, GST-NBC1EC4 and GST-AE1EC3 bound respectively 0.2 and 0.4 CAIV/GST, whereas GST-NBC1EC3 and GST alone bound only 0.02 and 0.03 CAIV/GST, respectively, when lysates of HEK293 cells expressing CAIV-WT were applied. Of interest, GST-NBC1EC4, GST-AE1EC4, and GST-NBC1EC3 binding to CAIV were only slightly higher than CAIV/GST binding (Fig. 6A, bottom), when lysates of HEK293 cells expressing CAIV-R69H mutant were used. Expression of CAIV-WT and CAIV-R69H proteins in cell lysates used for GST pull-down experiments was not different (Fig. 6B).

These results revealed that CAIV-WT binds specifically to EC4 of NBC1and EC4 of AE1, but CAIV-R69H mutant binding to EC4 of NBC1 and AE1 is critically impaired.

Colocalization of CAIV and NBC1 in Cells

Localization of GPI-anchored CAIV protein and NBC1 was assessed in HEK293 cells transiently cotransfected with wild-type CAIV or CAIV-R69H and NBC1 cDNAs. Wild-type CAIV and CAIV-R69H mutant had pericellular distribution (plasma membrane; Fig. 7A). NBC1 also mainly localized to the plasma membrane (Fig. 7A). Specificity of the CAIV and NBC1 signals was shown by the absence of signal in samples treated with secondary antibody and no primary antibody (not shown). The immunofluorescent behavior of two noninteracting plasma membrane proteins, the SLC26A6 chloride bicarbonate exchanger and the transferrin receptor, were also examined (Fig. 7B).

Quantitative analysis of colocalization of fluorescent signals revealed that CAIV-R69H/NBC1 overlapped significantly less

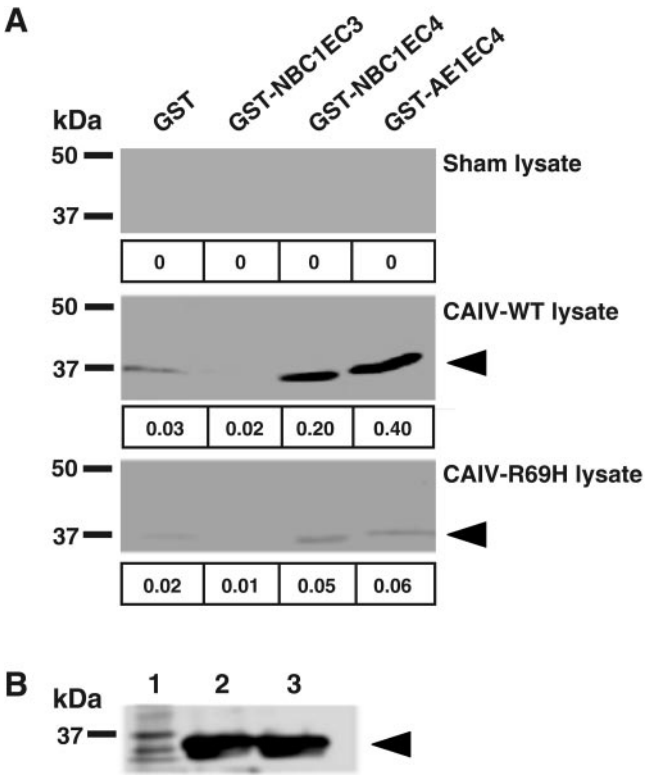

FIGURE 6. GST pull-down assays of the interaction of CAIV and R69H-CAIV with NBC1. (**A**) Protein (250 μg/lane of GST alone, GST-NBC1EC3, GST-NBC1EC4, and GST-AE1EC4) was bound to glutathione Sepharose 4B resin. Lysates of untransfected HEK293 cells (*top*), or HEK293 cells transfected with CAIV-WT cDNA (*middle*), or HEK293 cells transfected with CAIV-R69H mutant cDNA (*bottom*) were applied to the resin and incubated overnight. Eluted proteins were resolved by SDS-PAGE on 12% polyacrylamide gels, transferred to PVDF membrane, and probed for CAIV. The amount of CAIV in each lane was also quantified by densitometry. Parallel blots containing the same samples were probed for the amount of GST protein in each lane. Numbers at the bottom of each lane represent the amount of CAIV detected in that lane in relation to the amount of GST (pixels CAIV/pixels GST). (**B**) Expression of CAIV in lysates used for GST pull-down assays was measured on immunoblots probed with anti-human CAIV antibody: untransfected HEK293 cells (*lane 1*), CAIV-WT (*lane 2*), and CAIV-R69H (*lane 3*). *Arrows*: position of CAIV protein.

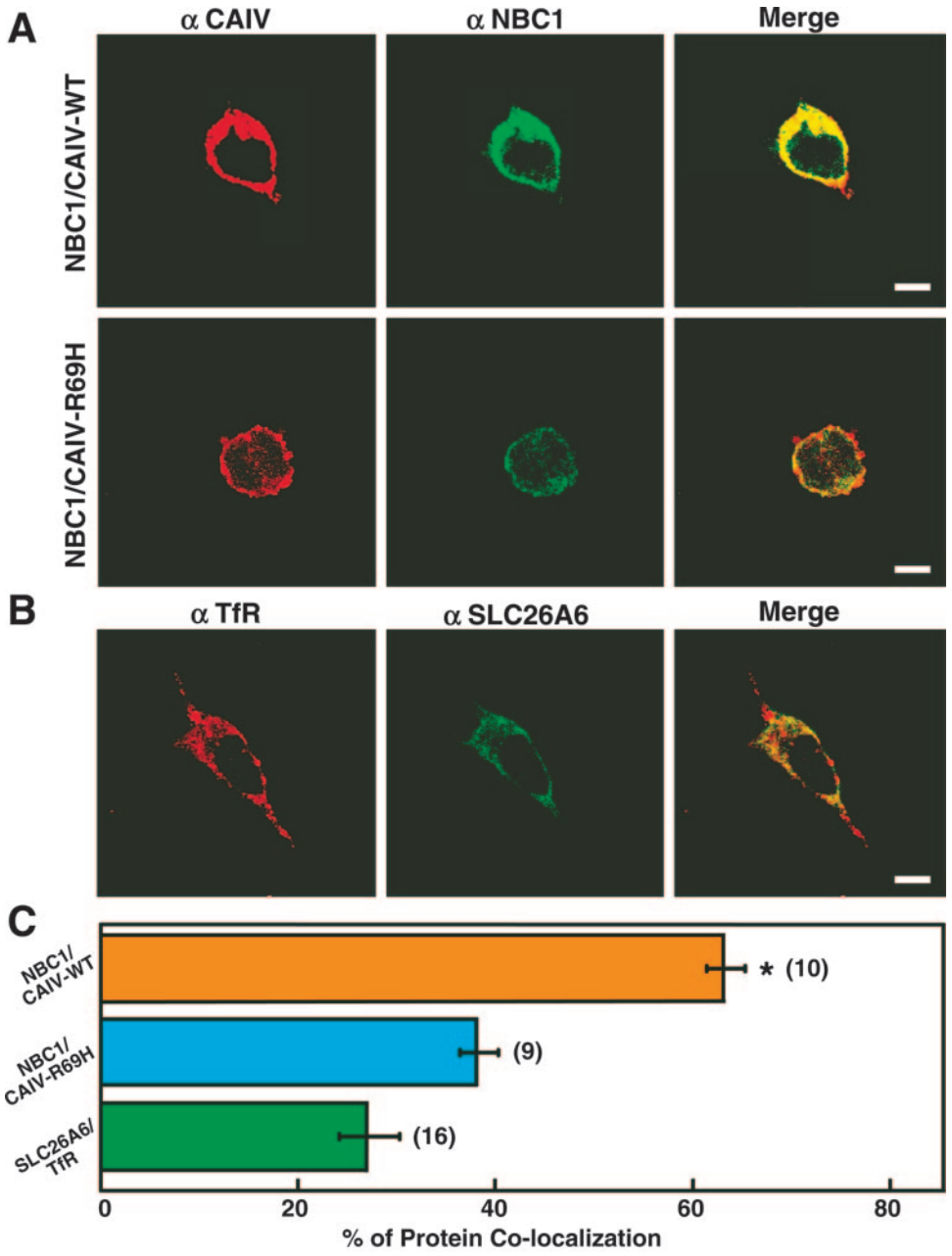

FIGURE 7. Colocalization of NBC1 and CAIV in transfected cells. HEK293 cells, cotransfected with NBC1 and CAIV wild-type or NBC1 and CAIV-R69H mutant, or transfected with human SLC26A6 cDNA, were plated on glass slides. (**A**) Transfected cells were stained with rabbit anti-NBC1 antibody, followed by Alexa Fluor 488–conjugated chicken anti-rabbit IgG secondary antibody (αNBC1, *green*) or with goat anti-CAIV antibody, followed by Alexa Fluor 594-conjugated chicken anti-goat IgG (αCAIV, *red*). Colocalization of CAIV wild-type or CAIV-R69H mutant and NBC1 is *yellow* (merge). (**B**) Images of cells stained with rabbit anti-SLC26A6 followed by Alexa Fluor 488–conjugated chicken anti-rabbit IgG secondary antibody (SLC26A6, *green*) or with goat anti-TfR antibody, followed by Alexa Fluor 594–conjugated chicken anti-goat IgG (TfR, *red*). Colocalization of SLC26A6 and TfR is *yellow* (merge). Images were collected with a laser scanning confocal microscope. Scale bar, 10 μm. (**C**) Images were analyzed to quantify the degree of CAIV-WT colocalization with NBC1 (*orange bar*), or CAIV-R69H and NBC1 (*blue bar*), or TfR and SLC26A6 (*green bar*). The number of cells is in brackets. $^*P < 0.05$.

(37% ± 2%) than did CAIV-WT/NBC1 colocalization (63% ± 2%; Fig. 7B, $P < 0.05$), suggesting that mutation in the CAIV protein affects the interaction between CAIV and NBC1. As expected, TfR localized to the plasma membrane, but colocalization with the membrane transporter SLC26A6 was only 27% ± 3%, indicating no association of these two proteins. Colocalization of NBC1/CAIV-R69H and SLC26A6/TfR showed a similar percentage of overlapping, by confocal microscopy studies. We conclude that interaction between NBC1 and the CAIV-R69H mutant in cellular membranes is dramatically reduced.

DISCUSSION

In this study, we identified a single mutation (R69H) in *CA4* in our analysis of 96 RP patients of Chinese ethnicity. The pathogenicity of this mutation is supported by the failure to observe this change in more than 400 ethnically matched control chromosomes and by the failure of the CAIV-R69H mutant to increase the NBC1-mediated rates of pH_i recovery after acid load, as had been observed with R14W and R219S mutations.[4] As direct interaction between CAIV and NBC1 is needed for the maximum rate of recovery of pH_i by NBC1, the R69H mutation must either abolish or decrease this physical interaction.

Protein modeling and hydrogen bond analysis of both native and mutant models (R219S and R69H) of CAIV revealed that R219 and R69 residues are linked by H-bond formation to a common residue, Gly103. The R129S mutation disrupts the hydrogen bonds Arg219 formed with Gly103. This diminished hydrogen bond network could distort the local tertiary structure of human carbonic anhydrase IV. Because R219 is located at the active cleft of the enzyme, this would lead to distortion of the catalytic center and may be the reason for the loss of CAIV enzymatic activity observed by Yang et al.[4] The modeled structure of R69H showed that His69 could still form a hydrogen bond with main chain atoms of Gly103, mimicking the

wild-type structure and thus preserving the local tertiary structure. Hence, the R69H mutation unlike R219S did not alter catalytic activity of CAIV. As our modeling will not take into account possible changes in hydrogen bonding that result from main chain atoms, all structural consequences of the R69H mutation to the loop with Gly103 cannot be determined.

The R69H mutation may, however, affect the tertiary structure of CAIV and thus interaction of CAIV with NBC1. CAIV is anchored to the plasma membrane by a GPI tail attached to its C terminus. This orientation is stabilized by interaction of 11 arginine, lysine, and histidine residues flanking the C terminus with the negatively charged phospholipid head groups of the membrane.[7] The Arg69 residue mutated in the Chinese patient with RP is one of the 11 residues responsible for the substantial electropositive surface potential surrounding the C terminus of CAIV. Although arginine and histidine are both classed as basic amino acids, histidine with its imidazole group has only a weak positive charge at neutral pH and therefore may not substitute well for arginine. The failure of R69H CAIV to interact with NBC1 in blot overlay and GST pull-down assays suggests the involvement of the region surrounding R69 in interaction with NBC1. The localization of R69 at the C-terminal end of a surface loop suggests an involvement of the loop in mediating CAIV/NBC1 interaction.

The human NBC1 gene (*SLC4A4*) encodes two electrogenic Na^+/HCO_3^- cotransport proteins, pNBC1 and kNBC1, that mediate electrogenic Na^+/HCO_3^- cotransport in ocular cells. In addition to choriocapillaris, pNBC1 is expressed in cornea, conjunctiva, lens, ciliary body, and in the inner retina (Müller cells), whereas the expression of kNBC1 is restricted to the conjunctiva.[14] Mutations in the coding region of the human NBC1 gene in exons common to both pNBC1 and kNBC1 cause a severe ocular phenotype, resulting in blindness, band keratopathy, glaucoma, and cataracts.[33–36] Mutations of NBC1 affect NBC1-mediated HCO_3^- transport,[33,34] or the processing of the NBC1 to the plasma membrane, therefore impairing the Na^+/HCO_3^- cotransport activity of NBC1.[35,36] The human kidney controls systemic pH in part by absorbing filtered bicarbonate in the proximal tubule via NBC1. Mutations of NBC1 caused proximal renal tubular acidosis in all cases. In some cases, NBC1 mutations resulted in other systemic defects, including short stature, mental retardation, poor dentition, and ataxia.

Mutations in *CA4* (R14W), which causes adRP on chromosome 17q22 (RP17), was first reported in a South African family.[3] In addition, several mutations in the *CA4* gene were simultaneously identified in other adRP families, confirming *CA4* as the RP17 gene.[4] We found that mutations of CAIV reduced NBC1 activity, yet we did not observe a renal phenotype, suggesting that the eye is more sensitive to loss of NBC1 activity than the kidney, possibly because of redundancy of CAs in the kidney proximal tubules and other tissues. Consistent with this, other RP17 patients with CAIV mutations did not present other systemic abnormalities.[3,4]

The retina is the most metabolically active tissue in the body, producing a substantial CO_2 load. Because the retina is poorly vascularized, efficient removal of metabolic by-products is key to normal ocular function. CO_2 produced by photoreceptors must be taken first by cells of the surrounding retinal pigmented epithelium before reaching the choriocapillaris. We found that CA4-R69H mutation encodes a functional carbonic anhydrase, but causes RP. CAIV and NBC1 colocalize in the choriocapillaris.[4] The failure of the R69H mutant to activate NBC1-mediated HCO_3^- flux fully suggests that the ability to funnel HCO_3^-/CO_2 through the choriocapillaris is a highly sensitive event. Coexpression of CAIV-WT and CAIV-R69H, mimicking the heterozygous state, supported NBC1 activity that was only slightly reduced relative to expression of CAIV-WT only, mimicking the homozygous-WT state. Thus, individuals in whom RP is caused by the CA4-R69H mutation have a small decrease in bicarbonate transport activity (and possibly a slightly more acid steady state pH_i, as suggested by data in Table 2), which nonetheless is sufficient to cause RP.

This proposed model explaining the effect of CAIV mutations contrasts with another that has been put forward[3] that proposes that impaired CAIV-R14W secretion, abnormal folding of the CAIV protein, and subsequent apoptotic cell death are responsible for photoreceptor degeneration. Our results describe an alternative pathogenic pathway in which a defect in the NBC1/CAIV functional complex involved in maintenance of pH balances and elimination of deleterious CO_2, leads to retinitis pigmentosa. Because we did not examine apoptosis that caused by the R69H CAIV mutation in our system, we cannot absolutely exclude increased apoptosis as the mechanism that triggers photoreceptor deterioration.

In conclusion, we have identified a novel mutation in *CA4* that provides further evidence that impaired pH regulation underlies photoreceptor degeneration in RP17. This study indicates that as with European patients with RP, mutations in *CA4* also account for ≤1% of cases of RP in Chinese patients.

Acknowledgments

The authors thank the patients for participating in the study.

References

1. Heckenlively J, Daiger S. Hereditary retinal and choroidal degenerations. In: Rimoin DI, Connor JM, Pyeritz RE, eds. *Principals and Practices of Medical Genetic.* 4th ed. New York: Churchill Livingston; 2001;2255–2576.
2. Daiger S. http://www.sph.uth.tmc.edu/RetNet/disease.htm/ provided in the public domain by the University of Texas Houston Health Science Center, Houston, TX; 2005.
3. Rebello G, Ramesar R, Vorster A, et al. Apoptosis-inducing signal sequence mutation in carbonic anhydrase IV identified in patients with the RP17 form of retinitis pigmentosa. *Proc Natl Acad Sci USA*. 2004;101:6617–6622.
4. Yang Z, Alvarez BV, Chakarova C, et al. Mutant carbonic anhydrase 4 impairs pH regulation and causes retinal photoreceptor degeneration. *Hum Mol Genet*. 2005;14:255–265.
5. Hageman GS, Zhu XL, Waheed A, Sly WS. Localization of carbonic anhydrase IV in a specific capillary bed of the human eye. *Proc Natl Acad Sci USA*. 1991;88:2716–2720.
6. Waheed A, Zhu XL, Sly WS. Membrane-associated carbonic anhydrase from rat lung purification characterization, tissue distribution and comparison with carbonic anhydrase IVs of other mammals. *J Biol Chem*. 1992;267:3308–3311.
7. Stams T, Nair SK, Okuyama T, Waheed A, Sly WS, Christianson DW. Crystal structure of the secretory form of membrane-associated human carbonic anhydrase IV at 2.8-A resolution. *Proc Natl Acad Sci USA*. 1996;93:13589–13594.
8. Bowne SJ, Sullivan LS, Blanton SH, et al. Mutations in the inosine monophosphate dehydrogenase 1 gene (IMPDH1) cause the RP10 form of autosomal dominant retinitis pigmentosa. *Hum Mol Genet*. 2002;11:559–568.
9. Chakarova CF, Hims MM, Bolz H, et al. Mutations in HPRP3, a third member of pre-mRNA splicing factor genes, implicated in autosomal dominant retinitis pigmentosa. *Hum Mol Genet*. 2002;11:87–92.
10. Kennan A, Aherne A, Palfi A, et al. Identification of an IMPDH1 mutation in autosomal dominant retinitis pigmentosa (RP10) revealed following comparative microarray analysis of transcripts derived from retinas of wild-type and Rho(−/−) mice. *Hum Mol Genet*. 2002;11:547–557.
11. McKie AB, McHale JC, Keen TJ, et al. Mutations in the pre-mRNA splicing factor gene PRPC8 in autosomal dominant retinitis pigmentosa (RP13). *Hum Mol Genet*. 2001;10:1555–1562.

12. Bonanno JA, Yi G, Kang XJ, Srinivas SP. Reevaluation of Cl^-/HCO3$^-$ exchange in cultured bovine corneal endothelial cells. *Invest Ophthalmol Vis Sci*. 1998;39:2713–2722.
13. Bok D, Galbraith G, Lopez I, et al. Blindness and auditory impairment caused by loss of the sodium bicarbonate cotransporter NBC3. *Nat Genet*. 2003;34:313–319.
14. Bok D, Schibler MJ, Pushkin A, et al. Immunolocalization of electrogenic sodium-bicarbonate cotransporters pNBC1 and kNBC1 in the rat eye. *Am J Physiol.* 2001;281:F920–F935.
15. Alvarez B, Loiselle FB, Supuran CT, Schwartz GJ, Casey JR. Direct extracellular interaction between carbonic anhydrase IV and the NBC1 Na^+/HCO_3^- co-transporter. *Biochemistry*. 2003;42:2321–2329.
16. Donner K, Hemila S, Kalamkarov G, Koskelainen A, Shevchenko T. Rod phototransduction modulated by bicarbonate in the frog retina: roles of carbonic anhydrase and bicarbonate exchange. *J Physiol*. 1990;426:297–316.
17. Marmor MF, Holder GE, Seeliger MW, Yamamoto S. Standard for clinical electroretinography (2004 update). *Doc Ophthalmol*. 2004;108:107–114.
18. Kaplan W, Littlejohn TG. Swiss-PDB Viewer (Deep View). *Brief Bioinform*. 2001;2:195–197.
19. Choi I, Romero MF, Khandoudi N, Bril A, Boron WF. Cloning and characterization of a human electrogenic Na^+-HCO_3^- cotransporter isoform (hhNBC). *Am J Physiol*. 1999;276:C576–C584.
20. Alvarez BV, Vilas GL, Casey JR. Metabolon disruption: a mechanism that regulates bicarbonate transport. *EMBO J*. 2005;24:2499–2511.
21. Sterling D, Alvarez BV, Casey JR. The extracellular component of a transport metabolon: Extracellular loop 4 of the human AE1 Cl^-/HCO_3^- exchanger binds carbonic anhydrase IV. *J Biol Chem*. 2002;277:25239–25246.
22. Maren TH. A simplified micromethod for the determination of carbonic anhydrase and its inhibitors. *J Pharmacol Exp Ther*. 1960;130:26–29.
23. Sundaram V, Rumbolo P, Grubb J, Strisciuglio P, Sly WS. Carbonic anhydrase II deficiency: diagnosis and carrier detection using differential enzyme inhibition and inactivation. *Am J Hum Genet*. 1986;38:125–136.
24. Sato S, Zhu XL, Sly WS. Carbonic anhydrase isozymes IV and II in urinary membranes from carbonic anhydrase II-deficient patients. *Proc Natl Acad Sci USA*. 1990;87:6073–6076.
25. Brion LP, Schwartz JH, Zavilowitz BJ, Schwartz GJ. Micro-method for the measurement of carbonic anhydrase activity in cellular homogenates. *Anal Biochem*. 1988;175:289–297.
26. Okuyama T, Sato S, Zhu XL, Waheed A, Sly WS. Human carbonic anhydrase IV: cDNA cloning, sequence comparison, and expression in COS cell membranes. *Proc Natl Acad Sci USA*. 1992;89:1315–1319.
27. Lohi H, Lamprecht G, Markovich D, et al. Isoforms of SLC26A6 mediate anion transport and have functional PDZ interaction domains. *Am J Physiol*. 2003;284:C769–C779.
28. Thompson JD, Higgins DG, Gibson TJ. CLUSTAL W: improving the sensitivity of progressive multiple sequence alignment through sequence weighting, position-specific gap penalties and weight matrix choice. *Nucleic Acids Res*. 1994;22:4673–4680.
29. Liang MP, Banatao DR, Klein TE, Brutlag DL, Altman RB. WebFEATURE: An interactive web tool for identifying and visualizing functional sites on macromolecular structures. *Nucleic Acids Res*. 2003;31:3324–3327.
30. Boron WF, De Weer P. Intracellular pH transients in squid giant axons caused by CO2, NH3, and metabolic inhibitors. *J Gen Physiol*. 1976;67:91–112.
31. Roos A, Boron WF. Intracellular pH. *Physiol Rev*. 1981;61:296–434.
32. Ch'en FF, Dilworth E, Swietach P, Goddard RS, Vaughan-Jones RD. Temperature dependence of Na^+-H^+ exchange, Na^+-HCO_3^- cotransport, intracellular buffering and intracellular pH in guinea-pig ventricular myocytes. *J Physiol*. 2003;552;715–726.
33. Igarashi T, Inatomi J, Sekine T, et al. Mutations in SLC4A4 cause permanent isolated proximal renal tubular acidosis with ocular abnormalities. *Nat Genet*. 1999;23:264–266.
34. Dinour D, Chang MH, Satoh J, et al. A novel missense mutation in the sodium bicarbonate cotransporter (NBCe1/SLC4A4) causes proximal tubular acidosis and glaucoma through ion transport defects. *J Biol Chem*. 2004;279:52238–52246.
35. Horita S, Yamada H, Inatomi J, et al. Functional analysis of NBC1 mutants associated with proximal renal tubular acidosis and ocular abnormalities. *J Am Soc Nephrol*. 2005;16:2270–2278.
36. Demirci FY, Chang MH, Mah TS, Romero MF, Gorin MB. Proximal renal tubular acidosis and ocular pathology: a novel missense mutation in the gene (SLC4A4) for sodium bicarbonate cotransporter protein (NBCe1). *Mol Vis*. 2006;12:324–330.